Supporting Information

Bioinspired strengthening and toughening carbon nanotube@polyaniline/graphene film using electroactive biomass as glue for high rate, volumetric capacitance and low-temperature tolerance flexible supercapacitor

Dan Wu,[ab] Chuying Yu[a] and Wenbin Zhong*[a]

[a]College of Materials Science and Engineering, Hunan University, Changsha, 410082, P. R. China

[b]College of Materials and Chemical Engineering, Hunan City University, Yiyang, 413000, P. R. China

*Corresponding author E-mail: wbzhong@hnu.edu.cn (W. Zhong).

Preparation of cellulose hydrogel

Firstly, microcrystalline cellulose (600 mg) and bacterial cellulose (18 mg) were added sequentially to 9.7 g precooled sodium hydroxide/urea/water (1 : 1.7 : 11, wt %) mixture under vigorous stirring to obtain a homogeneous viscous dispersion. The as-prepared viscous dispersion was poured into glass molds. Then 0.5 mol L^{-1} H_2SO_4 aqueous solution was slowly added to the viscous dispersion until the white cellulose hydrogel was formed. The obtained cellulose hydrogel was washed with excess water to remove residual chemicals before use.
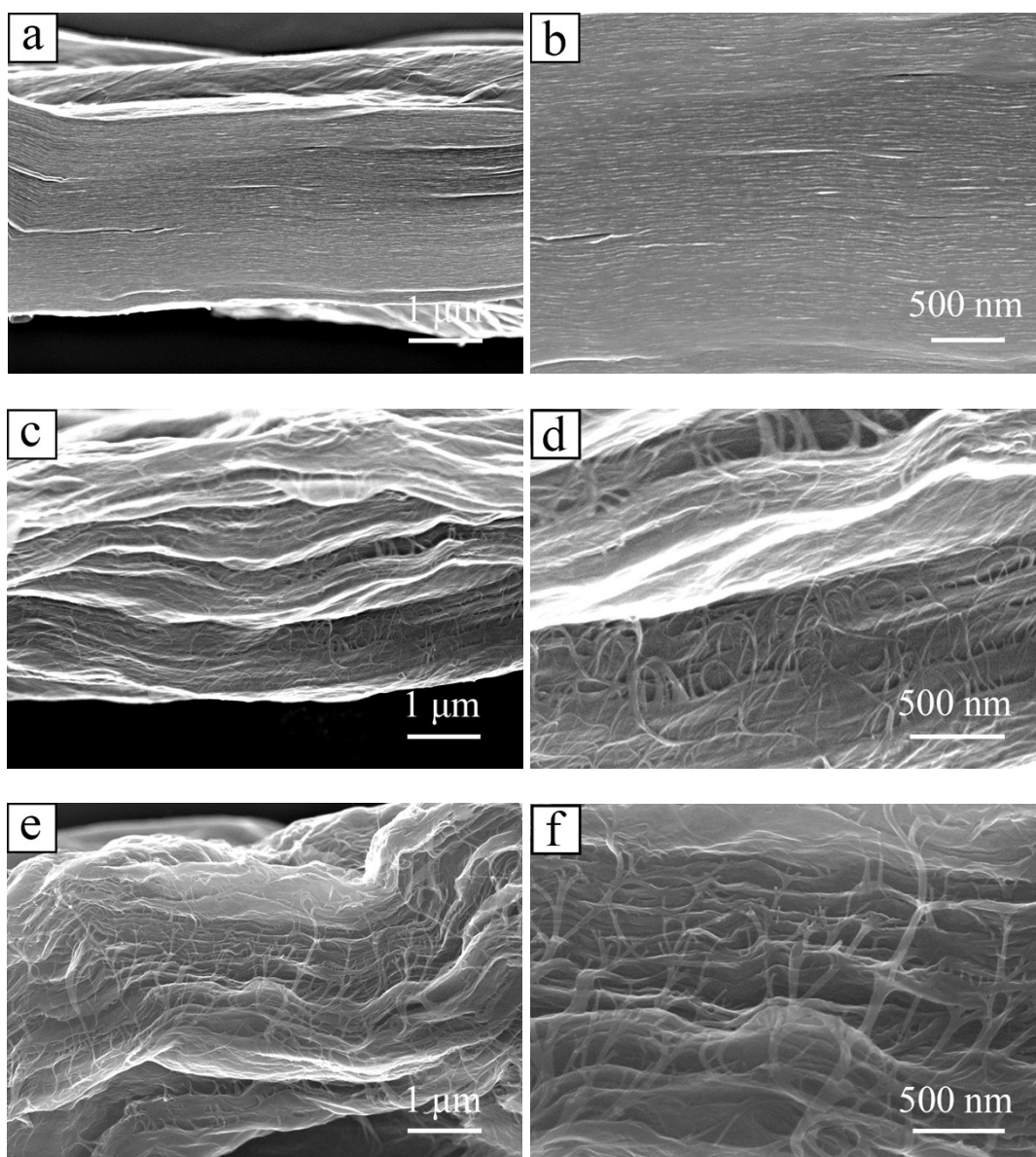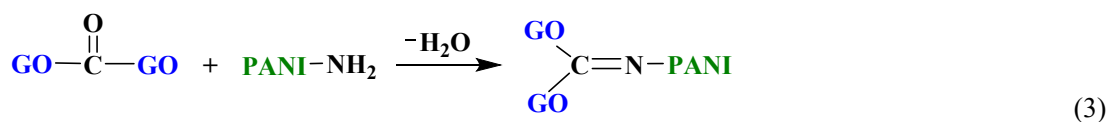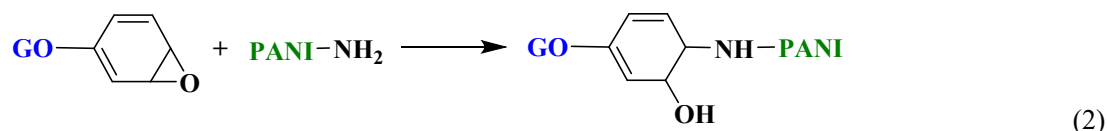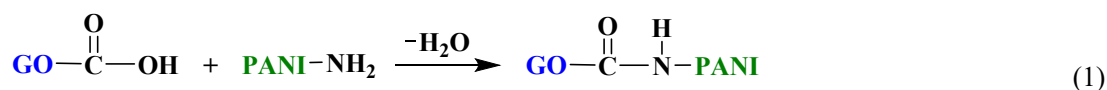
Figure S1. SEM images of the cross-section of (a, b) rGO, (c, d) CNT/rGO, and (e, f) CNT@PANI/rGO film in different resolution.
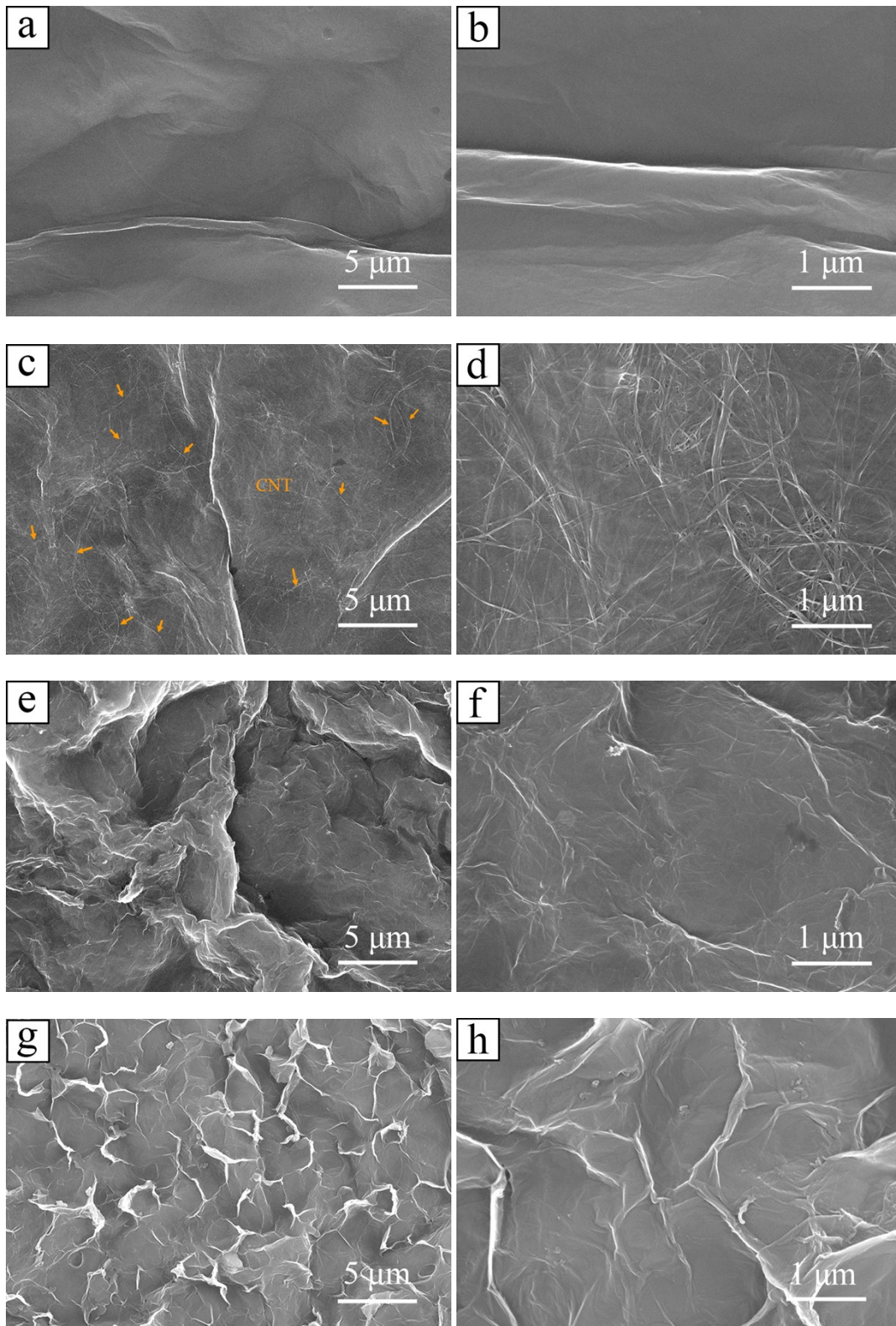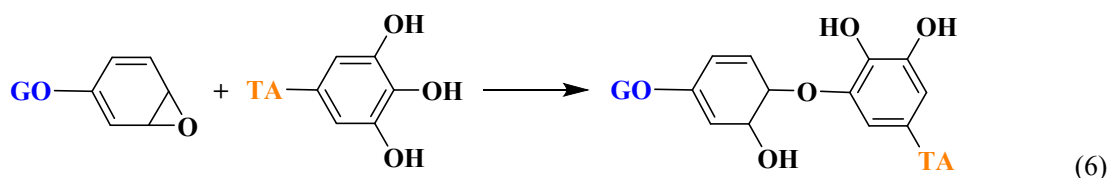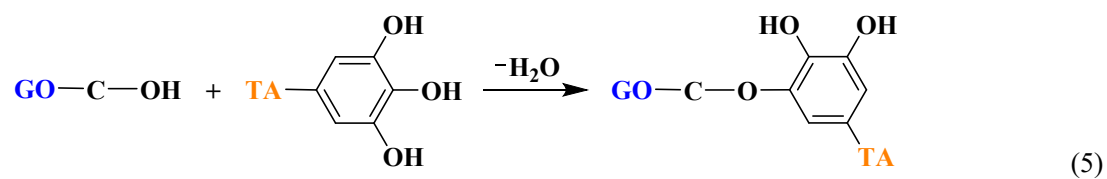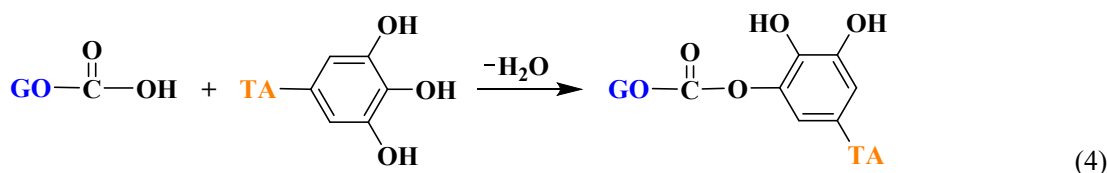
Figure S2. SEM images of the surface of (a, b) rGO, (c, d) CNT/rGO, (e, f) CNT@PANI/rGO, and (g, h) CNT@PANI/rGO/TA film in different resolution.
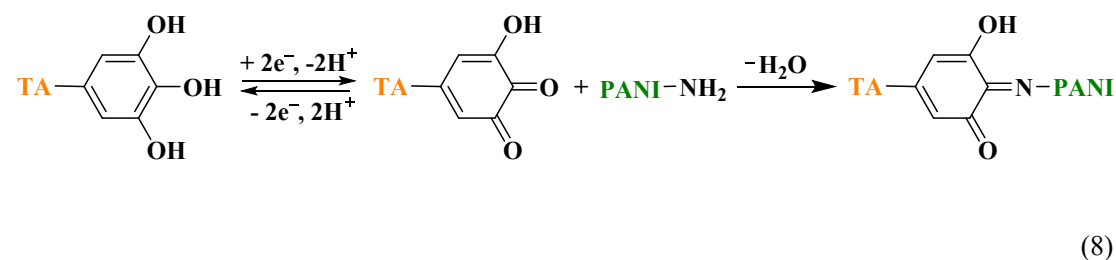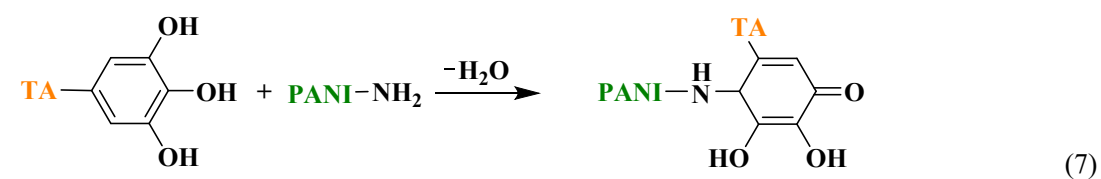
a. Chemical reactions between GO and PANI coated on the surface of CNT:

$$GO-\underset{\underset{O}{\|}}{C}-OH \; + \; PANI-NH_2 \; \xrightarrow{-H_2O} \; GO-\underset{\underset{O}{\|}}{C}-\overset{H}{N}-PANI \tag{1}$$

$$GO-\!\!\!\!<\!\!\text{epoxide}\!\!>\!\!\!\! \; + \; PANI-NH_2 \; \longrightarrow \; GO-\!\!\!\!<\!\!\text{ring}\!\!>\!\!-NH-PANI,\; OH \tag{2}$$

$$GO-\underset{\underset{O}{\|}}{C}-GO \; + \; PANI-NH_2 \; \xrightarrow{-H_2O} \; \underset{GO}{\overset{GO}{C}}\!=\!N-PANI \tag{3}$$

b. Chemical reactions between GO and TA:

$$GO-\underset{\underset{O}{\|}}{C}-OH \; + \; TA-\!\!<\!\!OH,OH,OH\!\!> \; \xrightarrow{-H_2O} \; GO-\underset{\underset{O}{\|}}{C}-O-\!\!<\!\!HO,OH\!\!>\!\!TA \tag{4}$$

$$GO-C-OH \; + \; TA-\!\!<\!\!OH,OH,OH\!\!> \; \xrightarrow{-H_2O} \; GO-C-O-\!\!<\!\!HO,OH\!\!>\!\!TA \tag{5}$$

$$GO-\!\!<\!\!\text{epoxide}\!\!> \; + \; TA-\!\!<\!\!OH,OH,OH\!\!> \; \longrightarrow \; GO-\!\!<\!\!\text{ring},OH\!\!>\!\!-O-\!\!<\!\!HO,OH\!\!>\!\!TA \tag{6}$$

c. Chemical reactions between TA and PANI coated on the surface of CNT:

$$TA-\!\!<\!\!OH,OH,OH\!\!> \; + \; PANI-NH_2 \; \xrightarrow{-H_2O} \; PANI-\overset{H}{N}-\!\!<\!\!TA,\,O;\,HO,OH\!\!> \tag{7}$$

$$TA-\!\!<\!\!OH,OH,OH\!\!> \; \underset{-2e^-,\,2H^+}{\overset{+2e^-,\,-2H^+}{\rightleftharpoons}} \; TA-\!\!<\!\!OH,O,O\!\!> \; + \; PANI-NH_2 \; \xrightarrow{-H_2O} \; TA-\!\!<\!\!OH,N-PANI,O\!\!> \tag{8}$$

Figure S3. Chemical reactions between (a) GO and PANI, (b) GO and TA, and (c) TA

and PANI.
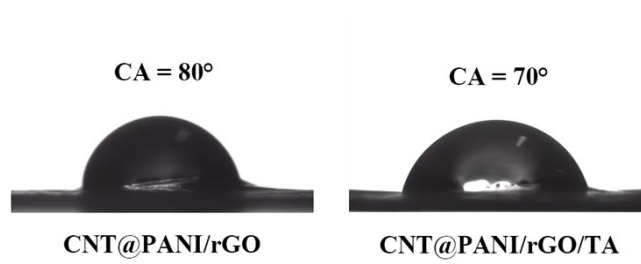
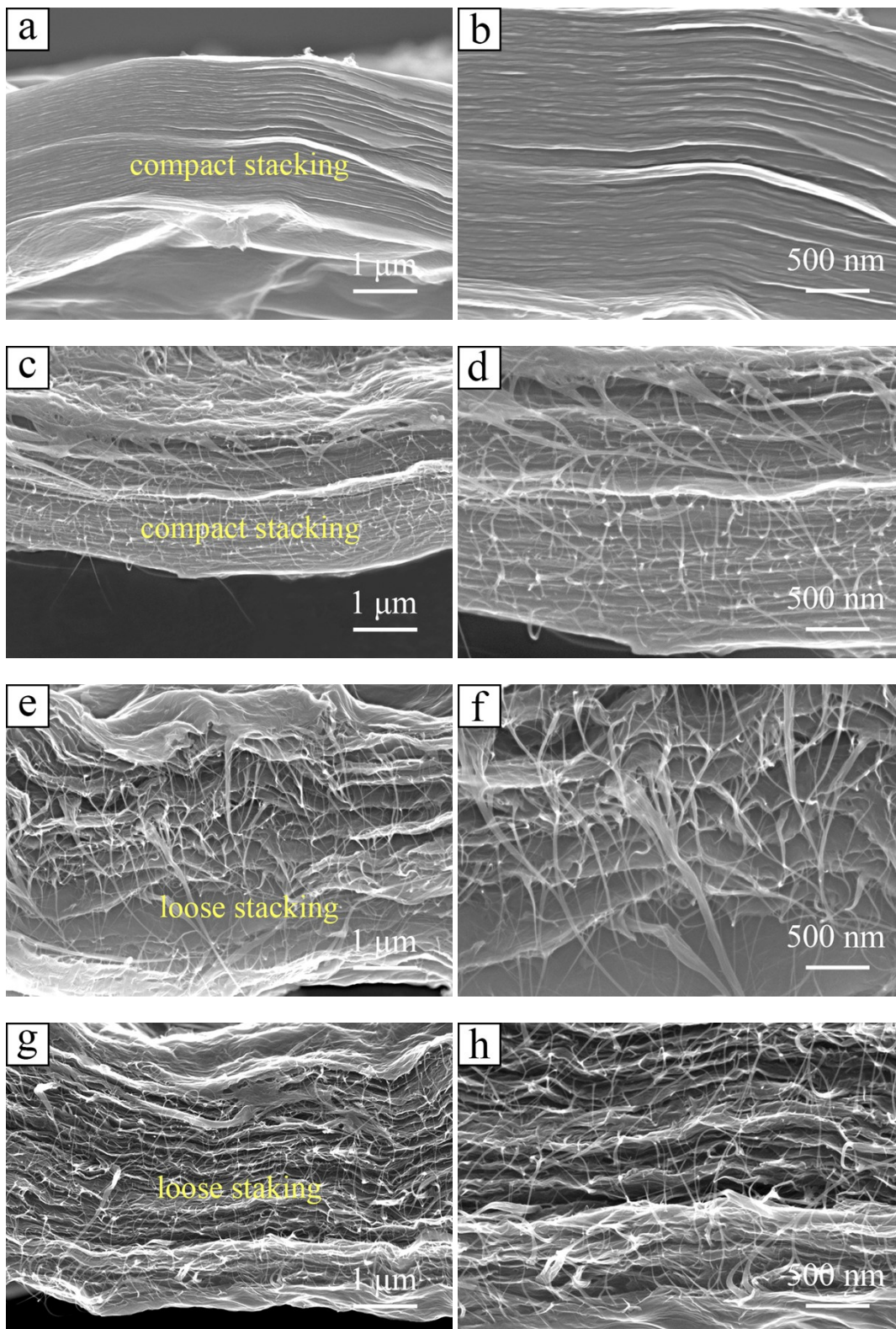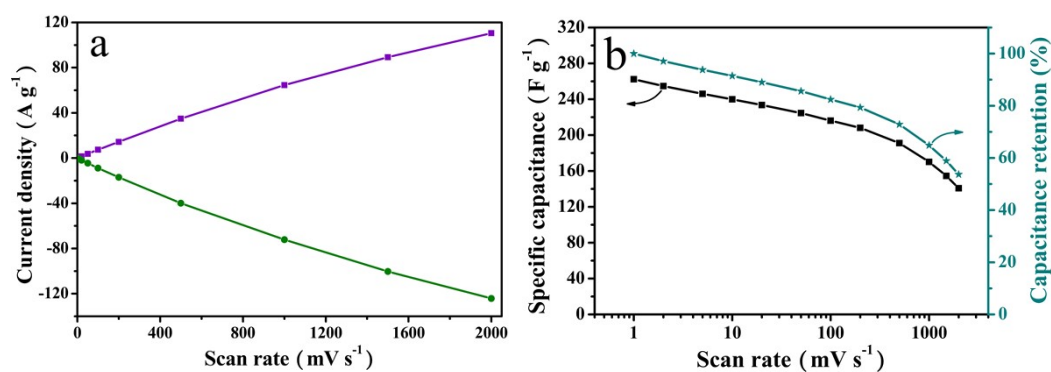**Figure S4.** Water contact angle measurements for CNT@PANI/rGO and CNT@PANI/rGO/TA film.

Figure S5. SEM images of the fracture surface of (a) rGO, (b) CNT/rGO, (c) CNT@PANI/rGO, and (d) CNT@PANI/rGO/TA film in different magnifications.

Figure S6. (a) The relationship between the maximum current density and scan rate based on CV curves and (b) the specific capacitance and the capacitance retention at different scan rate (1-2000 mV s^{-1}) for CNT@PANI/rGO/TA-based supercapacitor.
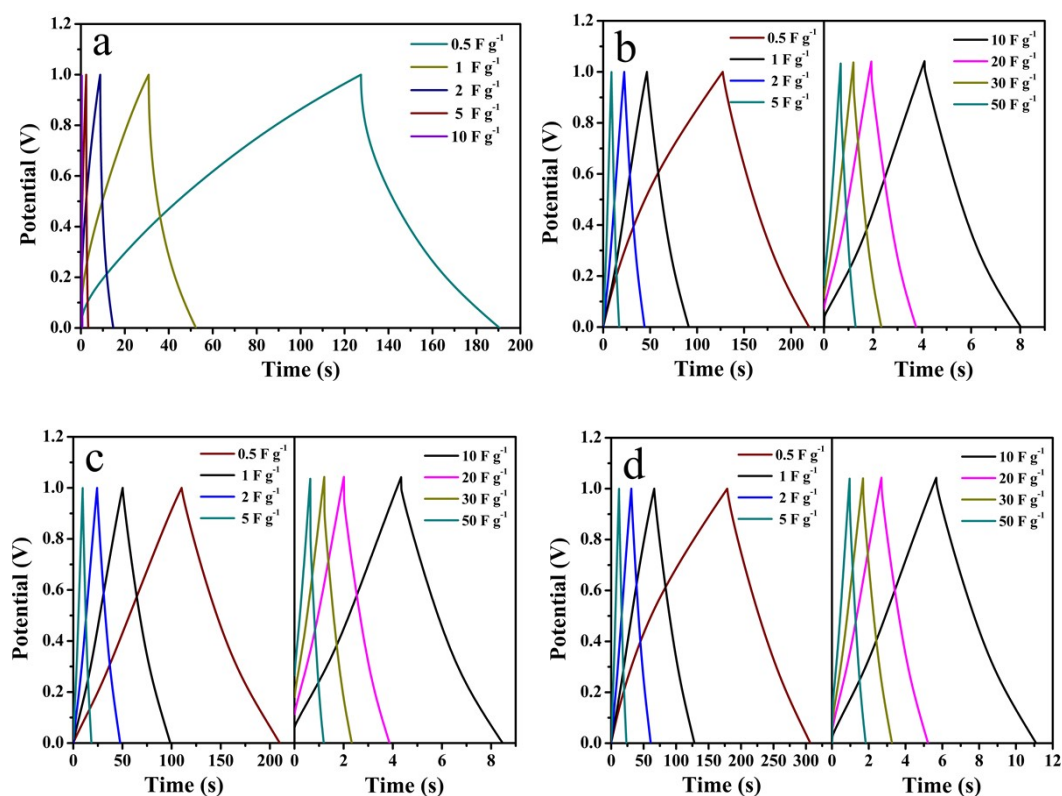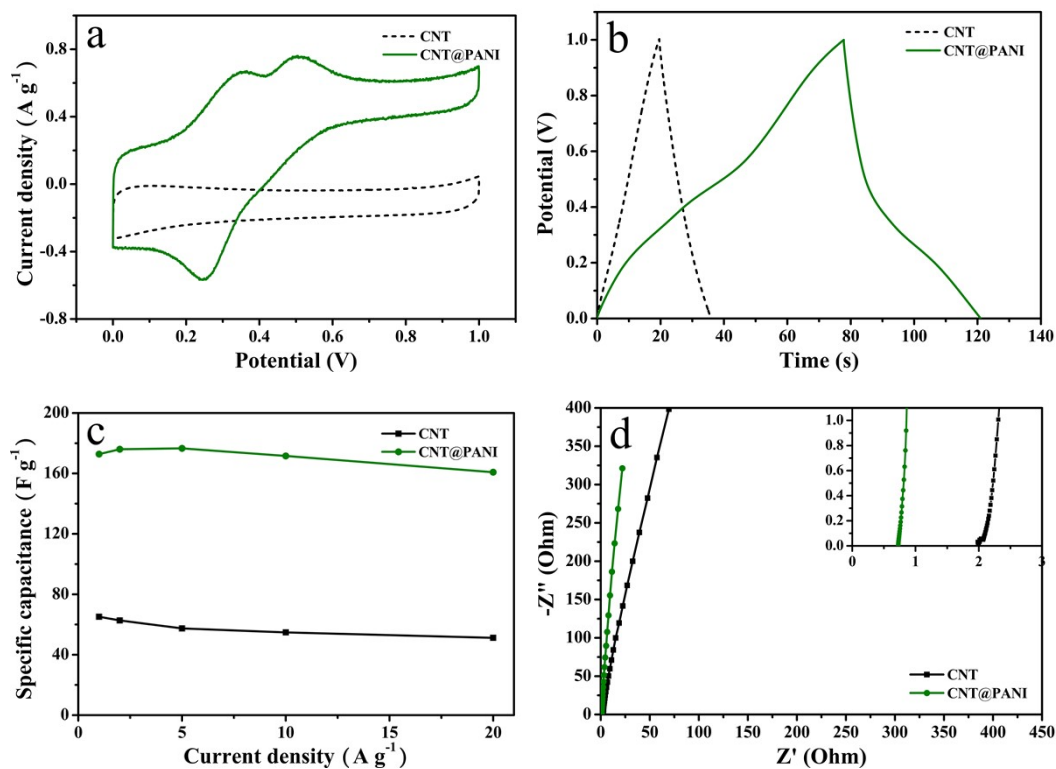

Figure S7. GCD curves of (a) rGO, (b) CNT/rGO, (c) CNT@PANI/rGO, and (d) CNT@PANI/rGO/TA at different current densities.

Figure S8. The electrochemical performance of the CNT@PANI and CNT electrodes in two-electrode system: (a) CV curves at a scan rate of 5 mV s^{-1}; (b) GCD curves at a current density of 1 A g^{-1}; (c) the specific capacitance *versus* different current densities (1 - 20 A g^{-1}); (d) Nyquist plots (the inset shows a magnified view of the high-frequency region).
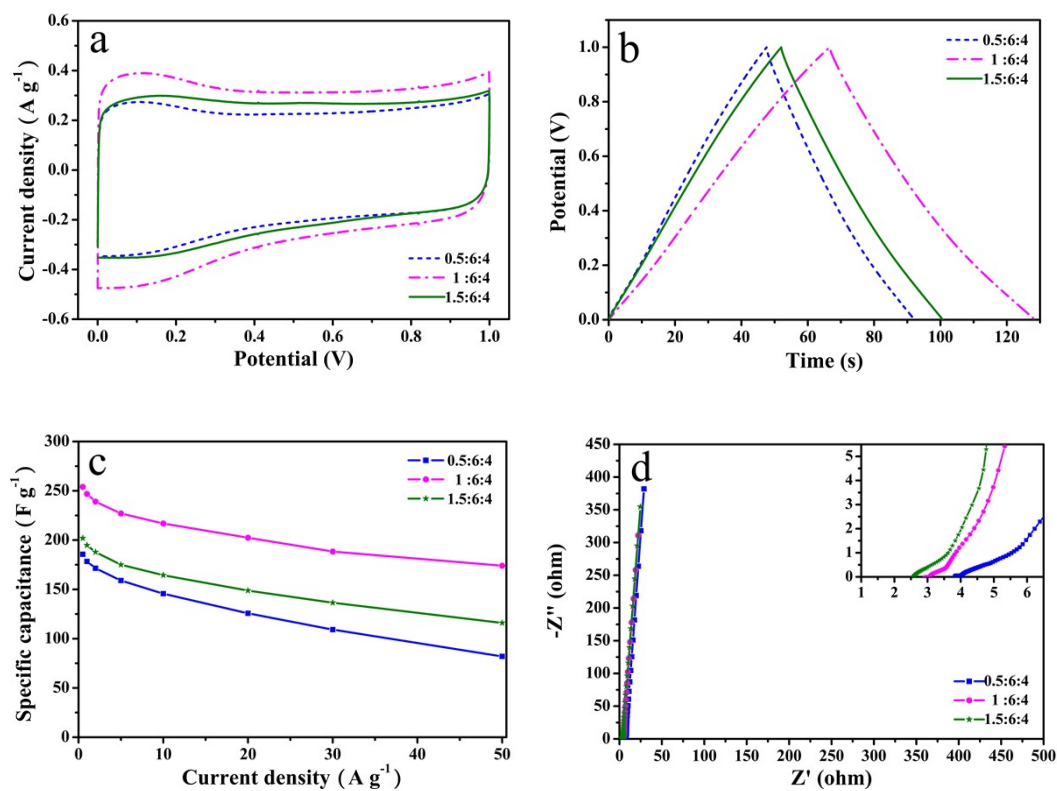
Figure S9. The electrochemical performance of the supercapacitor based on CNT@PANI/rGO/TA which prepared with different mass ratio of CNT@PANI to GO: (a) CV curves at a scan rate of 5 mV s^{-1}, (b) GCD curves at a current density of 1 A g^{-1}, (c) the specific capacitance *versus* different current densities (1-20 A g^{-1}), (d) Nyquist plots (the inset shows a magnified view of the high-frequency region).
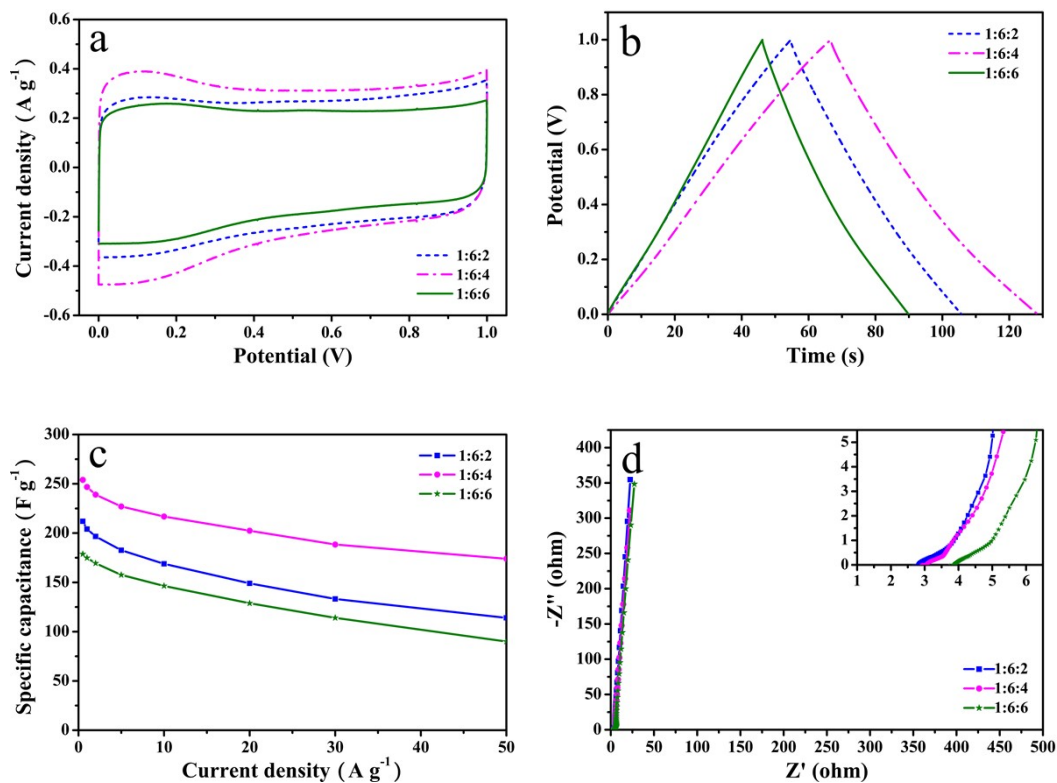
Figure S10. The electrochemical performance of the supercapacitor based on CNT@PANI/rGO/TA which prepared with different mass ratio of GO to TA: (a) CV curves at a scan rate of 5 mV s^{-1}, (b) GCD curves at a current density of 1 A g^{-1}, (c) the specific capacitance *versus* different current densities (1-50 A g^{-1}), (d) Nyquist plots (the inset shows a magnified view of the high-frequency region).
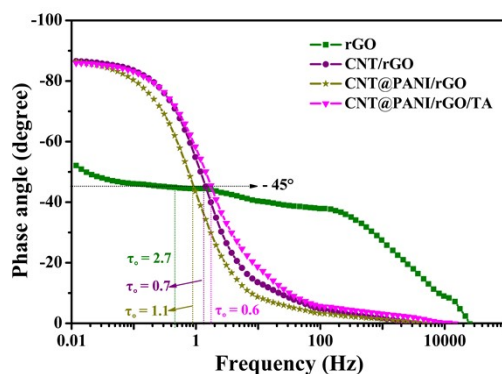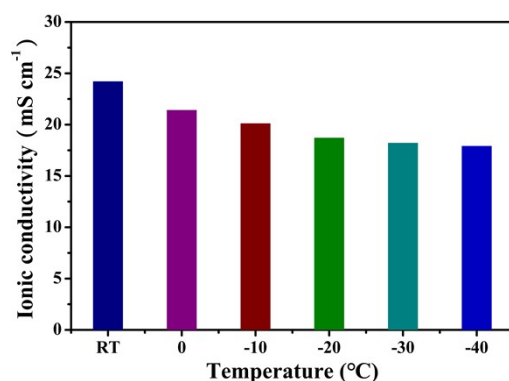
Figure S11. Bode plots of the all-solid-state supercapacitor with H_2SO_4/cellulose hydrogel electrolyte.

Figure S12. The ionic conductivity of organohydrogel electrolyte in the temperature range from room temperature to -40 °C. The ionic conductivity is calculated according to the formula: $\sigma = \dfrac{L}{R \times S}$. Where σ is the ionic conductivity; L is the distance between the two electrodes; R is the resistance of organohydrogel electrolytes; and S is the geometric area of the electrode/electrolyte interface.
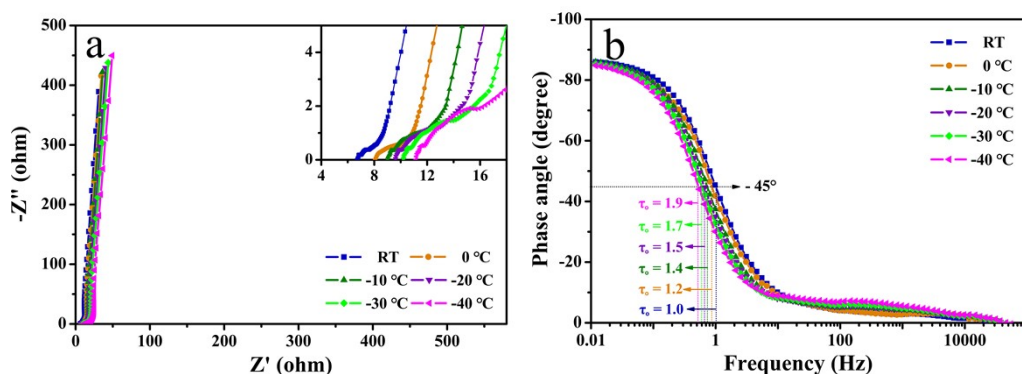
Figure S13. (a) Nyquist plots and (b) Bode plots of the all-solid-state supercapacitor with organohydrogel electrolyte.

Table S1. D-spacing (d), half peak width (FWHM) and degree (2θ) of rGO, CNT/rGO, CNT@PANI/rGO and CNT@PANI/rGO/TA.

Samples	d (Å)	FWHM	2θ (°)
rGO	3.83	7.47	23.2
CNT/rGO	3.83	7.00	23.2
CNT@PANI/rGO	3.91	7.70	22.7
CNT@PANI/rGO/TA	3.98	8.1	22.3

Table S2. The relative element contents (at %) of rGO, CNT/rGO, CNT@PANI/rGO and CNT@PANI/rGO/TA.

Samples	C	O	N
rGO	83.97	16.03	-
CNT/rGO	81.15	18.85	-
CNT@PANI/rGO	80.29	18.15	1.5
CNT@PANI/rGO/TA	81.45	17.02	1.48

Table S3. The relative content (at %) of N 1s species for CNT@PANI/rGO and CNT@PANI/rGO/TA.

Samples	-N=	-NH-	---NH$^+$---	-NH$^+$=
Binding energy (eV)	398.5	399.8	400.5	401.4
CNT@PANI/rGO	4.7	38.3	32.0	25.0
CNT@PANI/rGO/TA	0	37.8	38.2	24.0

Table S4. The electrical conductivity of different samples

Samples	Electrical conductivity (S cm^{-1})
rGO	21.7
CNT/rGO	200
CNT@PANI/rGO	111
CNT@PANI/rGO/TA	125

Table S5. Comparison of mechanical performance of the CNT@PANI/rGO/TA film with the reported graphene based films.

No.	Film	Preparation method	Strength (MPa)	Toughness (MJ m^{-3})	Reference
1	CNT@PANI/rGO/TA	Filtration	174.6	9.17	This work
2	rGO-MWCNT-PEDOT:PSS	Evaporation	252	7.3	[1]
3	PANI@halloysite/rGO	Filtration	351.9	8.5	[2]
4	rGO-PDA	Evaporation	204.9	4	[3]
5	rGO/ANF	Filtration	100.6	0.5	[4]
6	rGO- silk fibroin	Filtration	300	2.8	[5]
7	rGO-CNC-Mn^{2+}	Evaporation	475.2	6.6	[6]
8	rGO-MoS$_2$-TPU	Filtration	235.3	6.9	[7]
9	MXene/rGO	Filtration	379.2	14.2	[8]
10	MXene/rGO-AD	Filtration	699.1	42.7	[8]
11	rGO-DWNT-PCDO	Evaporation	374.1	9.2	[9]
12	rGO-MMT-PVA	Filtration	356	7.5	[10]
13	GO/PGA/Ca^{2+}	Evaporation	150		[11]

Table S6. Comparison of electrochemical performance of the CNT@PANI/rGO/TA based all-solid-state supercapacitor with the reported graphene based devices.

No.	Electrodes	Specific capacitance	Energy density (power density)	Capacitance retention (current density)	Reference
1	CNT@PANI/rGO/TA	548.6 F cm^{-3} (254 F g^{-1})	19.1 Wh L^{-1} (590 W L^{-1})	70.5 % (1 A g^{-1} to 50 A g^{-1}) 53.7 % (1 mV s^{-1} to 2000 mV s^{-1})	This work
2	DA/rGO@PDA	476.4 F cm^{-3} (277 F g^{-1})	16.3 Wh L^{-1} (218.8 W L^{-1})	71 % (0.5 A g^{-1} to 10 A g^{-1})	[12]
3	Graphene ribbon films	293 F cm^{-3} (318 F g^{-1})	11.5 Wh L^{-1} (82.7 W L^{-1})	~58.2 % (5 mA cm^{-2} to 105 mA cm^{-2})	[13]
4	Janus graphene films	127.7 F cm^{-3} (318 F g^{-1})	2.78 mWh cm^{-3} (40.3 mW cm^{-3})		[14]
5	rGO/CNT film	2 F cm^{-3} 330 mF cm^{-2}	1.7 mWh cm^{-3}	~84 % (0.1 mA cm^{-2} to 1 mA cm^{-2})	[15]
6	CNT/rGO fiber	54.9 F cm^{-3}	4.9 mWh cm^{-3} (15.5 W cm^{-3})		[16]
7	Unzipped CNT /rGO fiber	62.1 F cm^{-3} (45.6 F g^{-1})	8.63 mWh cm^{-3} (50.8 mW cm^{-3})	~67 % (0.1 A cm^{-3} to 4 A cm^{-3})	[17]
8	rGO/MXene fiber	345 F cm^{-3} (195 F g^{-1})	30.7 mWh cm^{-3} (70.7 mW cm^{-3})		[18]
9	PPDA-HGF film	516 F cm^{-3} (300 F g^{-1})	2.7 Wh L^{-1} (146.5 W L^{-1})	~80.1 % (1A g^{-1} to 20 A g^{-1})	[19]
10	POM-GFs film	115 F cm^{-3} (157 F g^{-1})	1.8 mWh cm^{-3} (398 mW cm^{-3})	~70.4 % (2 mV s^{-1} to 50 mV s^{-1})	[20]
11	PPD-graphene film	711 F cm^{-3}	15.4 Wh L^{-1} (380 W L^{-1})	~94.5 % (0.5A g^{-1} to 20 A g^{-1})	[21]
12	rGO/Ti$_3$C$_2$T$_x$ film	135.7 F cm^{-3} (148.5 F g^{-1})	2.3 Wh L^{-1} (67 W L^{-1})		[22]
13	Graphene flakes	200 F cm^{-3} (182 F g^{-1})	16 Wh L^{-1} (88 W L^{-1})		[23]
14	Holey graphene /PPy film	328 F cm^{-3}	22.3 Wh L^{-1} (189.5 W L^{-1})	~74 % (1 A g^{-1} to 20 A g^{-1})	[24]

15	PANI-graphene hydrogel film	572 F cm^{-3} (457.6 F g^{-1})	15.8 Wh L^{-1} (2800 W L^{-1})	~96 % (5 A g^{-1} to 100 A g^{-1})	25
16	N-containing graphene	586 F cm^{-3} (353 F g^{-1})	15.1 Wh L^{-1} (200 W L^{-1})	~80.6 % (5 A g^{-1} to 20 A g^{-1})	26
17	BPNOCNF film	395 F cm^{-3} (332 F g^{-1})	21.1 Wh L^{-1} (523.5 W L^{-1})	~80 % (1 A g^{-1} to 30 A g^{-1})	27

Some of the energy densities were calculated by the reported specific capacitance values.

Table S7. Comparison of low-temperature tolerance of the CNT@PANI/rGO/TA based device with the reported devices.

No.	Supercapacitors (electrode & electrolyte)	Specific capacitance (current density) at low temperature	Energy density (power density) at low temperature	Capacitance retention (low temperature vs RT)	Reference
1	CNT@PANI/rGO/TA & H_2SO_4 water/ ethylene glycol /PVA gel	454.9 F cm^{-3} 210.6 F g^{-1} (0.5 A g^{-1}) at -40 °C	15.8 W h L^{-1} ~7.3 W h kg^{-1} (250 W kg^{-1}) at -40 °C	87.6 % (-20 °C vs RT) 83.3 % (-40 °C vs RT)	This work
2	Graphene & $LiSO_4$/ethylene glycol/ water	74 F g^{-1} (1 mA cm^{-2}) at -20 °C	~2.57 W h kg^{-1} (500 μW cm^{-2}) at -20 °C	81.3 % (-20 °C vs RT)	28
3	N-Ti$_3$C$_2$Tx//HG2 & PVA/H_2SO_4 gel	84.5 F g^{-1} (0.5 A g^{-1}) at -20 °C	33.9 Wh kg^{-1} (425 W kg^{-1}) at -20 °C	~91.9 % (-20 °C vs RT)	29
4	AC & $LiClO_4$ water/glycerol/HPC /PVA gel	143.6 F g^{-1} (2 A g^{-1}) at -40 °C	16.2 Wh kg^{-1} (1800 W kg^{-1}) at -40 °C	73.75 % (-40 vs 20 °C)	30
5	CNT paper & LiCl H_2O/ethylene glycol/PVA gel	~25 mF cm^{-2} (1 mA cm^{-2}) at -40 °C		70.6 % (-40 vs 20 °C)	31
6	Gaphene/PEDOT /PVA fiber & H_2SO_4 H_2O/ ethylene glycol/ glycerol/PVA gel	212.6 F g^{-1} (0.1 A g^{-1}) at -20 °C	~4.7 Wh kg^{-1} (40 W kg^{-1}) at -20 °C	75.6 % (-20 vs 25 °C)	32
7	CNT film & H_2SO_4/PVA	0.74 mF cm^{-2} (0.2 mA cm^{-2}) at -5 °C		80.4 % (-5 vs 25 °C)	33
8	PANI/organohydrogel PAM polyelectrolyte (integrated supercapacitor)	~10.8 mF cm^{-2} (0.03 mA cm^{-2}) at -30 °C		~75 % (-30 °C vs RT)	34
9	Biochar-rGO & KOH/polyampholyte hydrogel	75 F g^{-1} (1 A g^{-1}) at -30 °C	~2.6 Wh kg^{-1} (500 W kg^{-1}) at -30 °C	42.9 % (-30 vs 20 °C)	35

10	MWCNT/HRGO/CF film & BMIMBF$_4$ electrolyte	23.9 F g^{-1} (10 mA cm^{-2}) at -30 °C	~10.2 Wh kg^{-1} (17500 W kg^{-1}) at -30 °C	~ 32 % (-30 *vs* 30 °C)	36
11	MXene-knotted carbon nanotube//AC & EMIM-TFSI/ACN	11 F g^{-1} (20 mV s^{-1}) at -60 °C		~55 % (-60 °C *vs* RT)	37
12	AC & CAN/DIOX	164 F g^{-1} (5 mV s^{-1}) at -100 °C		~94.8 % (-100 *vs* 20 °C)	38
13	AC & ACN/MF with SBP-BF$_4$ salt	66 F cm^{-3} 173 F g^{-1} (5 mV s^{-1}) at -100 °C	8.8 Wh kg^{-1} (3800 W kg^{-1}) at -100 °C		39
14	MWCNT-PANI films & MGO-PAM	141.7 F g^{-1} (0.5 A g^{-1}) at -30 °C		~84.7 % (-30 °C *vs* RT)	40
15	Graphene nanoplatelets & BMImCl/H$_2$O	166.4 F g^{-1} (20 mV s^{-1}) at -20 °C	36 Wh kg^{-1} (870 W kg^{-1}) at -20 °C	~33.8 % (-20 °C *vs* RT)	41
16	Templated carbon MP98B & IL electrolyte	37 F cm^{-3} 83 F g^{-1} (0.1 A g^{-1}) at -40 °C	6.3 Wh kg^{-1} (1000 W kg^{-1}) at -40 °C	~71.3 % (-40 °C *vs* RT)	42
17	Carbon & Acetone/H$_2$O 1 mol/L Mg(NO$_3$)$_2$	~28 F g^{-1}		~50 % (-40 °C *vs* RT)	43
18	AC & PAM-PVP-H$_3$PO$_4$	17.4 F g^{-1} (0.1 A g^{-1}) at -40 °C		~30 % (-40 °C *vs* RT)	44
19	Porous carbon & DMSO/H$_2$O LiTFSI	22.3 F g^{-1} (1 A g^{-1}) at -35 °C		~33.3 % (-35 *vs* 25 °C)	45

References

1 M. M. Islam, S. H. Aboutalebi, D. Cardillo, H. K. Liu, K. Konstantinov and S. X. Dou, *ACS Cent. Sci.*, 2015, **1**, 206-216.

2 C. Wu, T. Zhou, Y. Du, S. Dou, H. Zhang, L. Jiang and Q. Cheng, *Nano Energy*, 2019, **58**, 517-527.

3 W. Cui, M. Li, J. Liu, B. Wang, C. Zhang, L. Jiang and Q. Cheng, *ACS Nano*, 2014, **8**, 9511-9517.

4 S. R. Kwon, J. Harris, T. Zhou, D. Loufakis, J. G. Boyd and J. L. Lutkenhaus, *ACS Nano*, 2017, **11**, 6682-6690.

5 K. Hu, L. S. Tolentino, D. D. Kulkarni, C. Ye, S. Kumar and V. V. Tsukruk, *Angew. Chem. Int. Ed.*, 2013, **52**, 13784-13788.

6 S. Gong, Q. Zhang, R. Wang, L. Jiang and Q. Cheng, *J. Mater. Chem. A*, 2017, **5**, 16386-16392.

7 S. Wan, Y. Li, J. Peng, H. Hu, Q. Cheng and J. Lei, *ACS Nano*, 2015, **9**, 708-714.

8 T. Zhou, C. Wu, Y. Wang, A. P. Tomsia, M. Li, E. Saiz, S. Fang, R. H. Baughman, L. Jiang and Q. Cheng, *Nat. Commun.*, 2020, **11**, 2077.

9 S. Gong, W. Cui, Q. Zhang, A. Cao, L. Jiang and Q. Cheng, *ACS Nano*, 2015, **9**, 11568-11573.

10 P. Ming, Z. Song, S. Gong, Y. Zhang, J. Duan, Q. Zhang, L. Jiang and Q. Cheng, *J. Mater. Chem. A*, 2015, **3**, 21194-21200.

11 K. Liang, E. M. Spiesz, D. T. Schmieden, A.-W. Xu, A. S. Meyer and M.-E. Aubin-Tam, *ACS Nano*, 2020, **14**, 14731-14739.

12 C. Huang, Q. Tang, Q. Feng, Y. Li, Y. Xu, Y. Zhang, A. Hu, S. Zhang, W. Deng and X. Chen, *J. Mater. Chem. A*, 2020, **8**, 9661-9669.

13 L. Sheng, J. Chang, L. Jiang, Z. Jiang, Z. Liu, T. Wei and Z. Fan, *Adv. Funct. Mater.*, 2018, **28**, 1800597.

14 Z. Song, Y. Fan, Z. Sun, D. Han, Y. Bao and L. Niu, *J. Mater. Chem. A*, 2017, **5**, 20797-20807.

15 X. Zang, R. Zhang, Z. Zhen, W. Lai, C. Yang, F. Kang and H. Zhu, *Nano Energy*, 2017, **40**, 224-232.

16 W. Ma, M. Li, X. Zhou, J. Li, Y. Dong and M. Zhu, *ACS Appl. Mater. Interfaces*, 2019, **11**, 9283-9290.

17 W. Ma, W. Li, M. Li, Q. Mao, Z. Pan, J. Hu, X. Li, M. Zhu and Y. Zhang, *Adv. Funct. Mater.*, 2021, **31**, 2100195.

18 Z. Wang, Y. Chen, M. Yao, J. Dong, Q. Zhang, L. Zhang and X. Zhao, *J. Power Sources*, 2020, **448**, 227398.

19 X. Ye, Y. Zhu, H. Jiang, Z. Yue, L. Wang, Z. Wan and C. Jia, *J. Power Sources*, 2019, **441**, 227167.

20 S. Wang, X. Wang, C. Sun and Z.-S. Wu, *J. Energy Chem.*, 2021, **61**, 23-28.

21 G. Lian, C.-C. Tuan, L. Li, S. Jiao, K.-S. Moon, Q. Wang, D. Cui and C.-P. Wong, *Nano Lett.*, 2017, **17**, 1365-1370.

22 S. Xu, G. Wei, J. Li, W. Han and Y. Gogotsi, *J. Mater. Chem. A*, 2017, **5**, 17442-17451.

23 X. Peng, H. Cao, Z. Qin, C. Zheng, M. Zhao, P. Liu, B. Xu, X. Zhou, Z. Liu and J.

Guo, *Electrochim. Acta*, 2019, **305**, 56-63.

24 Z. Fan, J. Zhu, X. Sun, Z. Cheng, Y. Liu and Y. Wang, *ACS Appl. Mater. Interfaces*, 2017, **9**, 21763-21772.

25 Y. Wang, X. Yang, A. G. Pandolfo, J. Ding and D. Li, *Adv. Energy Mater.*, 2016, **6**, 1600185.

26 D. Wang, W. Hu, Q. Ma, X. Zhang, X. Xia, H. Chen and H. Liu, *Carbon*, 2019, **154**, 13-23.

27 Y. Ma, X. Zhang, Z. Liang, C. Wang, Y. Sui, B. Zheng, Y. Ye, W. Ma, Q. Zhao and C. Qin, *Electrochim. Acta*, 2020, **337**, 135800.

28 R. Vellacheri, A. Al-Haddad, H. Zhao, W. Wang, C. Wang and Y. Lei, *Nano Energy*, 2014, **8**, 231-237.

29 Q. Sun, T. He and Y. Li, *J. Mater. Chem. A*, 2020, **8**, 1687-1696.

30 N. Lu, R. Na, L. Li, C. Zhang, Z. Chen, S. Zhang, J. Luan and G. Wang, *ACS Appl. Mater. Interfaces*, 2020, **3**, 1944-1951.

31 Q. Rong, W. Lei, J. Huang and M. Liu, *Adv. Energy Mater.*, 2018, **8**, 1801967.

32 T. Xu, D. Yang, S. Zhang, T. Zhao, M. Zhang and Z.-Z. Yu, *Carbon*, 2021, **171**, 201-210.

33 D.-Z. Chen, J. Yu, W. Lu, Y. Zhao, Y. Yan and T.-W. Chou, *Electrochim. Acta*, 2017, **233**, 181-189.

34 X. Jin, L. Song, H. Yang, C. Dai, Y. Xiao, X. Zhang, Y. Han, C. Bai, B. Lu, Q. Liu, Y. Zhao, J. Zhang, Z. Zhang and L. Qu, *Energy Environ. Sci.*, 2021, **14**, 3075-3085.

35 X. Li, L. Liu, X. Wang, Y. S. Ok, J. A. W. Elliott, S. X. Chang and H.-J. Chung, *Sci.*

Rep., 2017, **7**, 1685.

36 Y. Yang, S. W. Ng, D. Chen, J. Chang, D. Wang, J. Shang, Q. Huang, Y. Deng and Z. Zheng, *Small*, 2019, **15**, 1902071.

37 X. Gao, X. Du, T. S. Mathis, M. Zhang, X. Wang, J. Shui, Y. Gogotsi and M. Xu, *Nat. Commun.*, 2020, **11**, 6160.

38 J. Xu, N. Yuan, J. M. Razal, Y. Zheng, X. Zhou, J. Ding, K. Cho, S. Ge, R. Zhang, Y. Gogotsi and R. H. Baughman, *Energy Storage Mater.*, 2019, **22**, 323-329.

39 X. Wang, J. Xu, J. M. Razal, N. Yuan, X. Zhou, X. Wang, J. Ding, S. Qin, S. Ge and Y. Gogotsi, *J. Mater. Chem. A*, 2019, **7**, 16339-16346.

40 X. Jin, G. Sun, G. Zhang, H. Yang, Y. Xiao, J. Gao, Z. Zhang and L. Qu, *Nano Research*, 2019, **12**, 1199-1206.

41 A. Tatlisu, Z. Huang and R. Chen, *ChemSusChem*, 2018, **11**, 3899-3904.

42 E. Pameté Yambou, B. Gorska, V. Pavlenko and F. Beguin, *Electrochim. Acta*, 2020, **350**, 136416.

43 J. Menzel, E. Frackowiak and K. Fic, *J. Power Sources*, 2019, **414**, 183-191.

44 M. Wang, L. Fan, G. Qin, X. Hu, Y. Wang, C. Wang, J. Yang and Q. Chen, *J. Membr. Sci.*, 2020, **597**, 117740.

45 X. Lu, R. J. Jimenez-Rioboo, D. Leech, M. C. Gutierrez, M. L. Ferrer and F. Del Monte, *ACS Appl. Mater. Interfaces*, 2020, **12**, 29181-29193.